**Ping He[1,*], Haoran Jin[1], Mingming Zheng[1] Runjie Shen[2]**

J. Electrical Systems 18-2 (2022): 173-192

**Regular paper**


# Coordinated design of PSS and multiple FACTS devices based on the improved steepest descent algorithm to improve the small-signal stability of wind-PV grid-connected system

The integration of renewable energy has a significant impact on the stability of the power system, especially the unpredictable threat on the small-signal stability. The flexible AC transmission system (FACTS) devices can quickly adjust the fundamental wave power flow to improve the transmission capacity and stability of power systems. This paper proposes an improved steepest descent algorithm (SDA) to coordinate and optimize the control parameters of PSS, TCSC and UPFC-PODC, the initial values and ranges of parameters are determined by the critical eigenvalue locus movement (ELM). Extensive simulations on the eight machines twenty-four buses power system verify the effectiveness of the proposed method on improving the damping level and restraining the low frequency oscillation.

Keywords: wind-PV grid-connected power generation, low frequency oscillation, PSS, FACTS devices, coordinated optimization.

## 1. Introduction

Renewable energies show superiorities on alleviating the energy crisis and reducing environmental pollution[1, 2] and have been widely integrated into the power system. However, the large amount integration of wind and photovoltaic (PV) energies [3] brings new challenges to the reliability and stability of power systems[4], especially, small-signal stability issues. For instance, electromechanical oscillations with the frequency of about 0.1-2.5Hz occurring in the power system are regarded as low frequency oscillations (LFO)[5, 6], which is an important indicator for measuring the small-signal stability of the system. Continuous oscillations will limit the transmission capacity of the transmission line. More seriously, it may cause the system to be disconnected and has a huge impact on the stability of the system.

In order to suppress the LFO of the power system, cost-effective methods have been studied, including the installation of PSS on the generator[7]. PSS usually generates a positive damping torque in the generator excitation circuit to offset the negative damping torque generated in the original excitation voltage regulator, thereby improving the system damping level and enhancing the dynamic stability of the system [8, 9]. But in the large-scale area interconnected power system with more generators, the traditional PSS may sometimes fail to provide sufficient damping in areas where LFO needs to be suppressed [10].

On the other hand, the rapid development of flexible AC transmission system (FACTS) play an important role in increasing the transmission capacity of the transmission line, adjusting the power flow distribution of the power grid, and damping the LFO of the

* Corresponding author: Ping He, College of Electric and Information Engineering, Zhengzhou University of Light Industry, Zhengzhou; Henan, China, E-mail: hplkz@126.com
[1] College of Electric and Information Engineering, Zhengzhou University of Light Industry, Zhengzhou; Henan, China
[2] State Grid Shanxi Province Electric Power Company Changzhi Power Supply Company, Changzhi, Shanxi, China

system [11, 12]. Thyristor controlled series compensation (TCSC) changes the impedance value of the line according to the change of the control signal (such as line power) and adjusts the power flow distribution of the system. When TCSC is used for power modulation, the compensation degree of TCSC can be changed according to the selected auxiliary signal, the transmission power of the transmission line can be changed, and the LFO of the power system can be suppressed [13, 14]. With its powerful functions, unified power flow controller (UPFC) can greatly change the power flow of transmission lines, improve system damping, suppress LFO, and enhance the dynamic stability of the power system [15]. Moreover, the additional damping control based on FACTS devices has also been extensively researched, especially in terms of damping inter-area oscillations, it has a more flexible control method and faster response speed than traditional damping control. The additional power oscillation damping controller (PODC) can provide sufficient damping torque, effectively suppress the LFO of the system, and improve the stability of the system [16].

However, studies have shown that when different controllers coexist in the power system, they will interact with each other, that is, once there is an inappropriate setting of the controller parameters, different types of controllers may reduce the system damping or will even exacerbate system oscillation [17]. Hence, it is increasingly important to study the coordinated optimization between PSS and FACTS devices. Reference [18] proposed a method combining continuous wavelet transform and Prony algorithm to coordinate and optimize the parameters of PSS and UPFC, effectively suppressing the LFO of the power system. Reference [19] applied a particle swarm optimization algorithm that can search for the L and C values of Static Var Compensator (SVC) to achieve fine coordination of SVC and TCSC parameters. The results show that through coordination and optimization, the stability of the system can be significantly improved. Reference [20] studied the influence of PSS and static series synchronous compensator (SSSC) on the stability of DFIG wind power system, designed an objective function related to rotor speed deviation, and coordinated and optimized the compensation degree of SSSC and the gain of PSS. The results show that by optimizing the parameters of controllers, the oscillation in the system can be suppressed to the greatest extent. Reference [21] proposed a system identification estimator based on artificial neural network, which can identify the equivalent transfer function of the wind power system in real time. And adopt the depth deterministic strategy gradient algorithm to realize the adaptive robust control strategy of static synchronous compensator having additional damper controller. Reference [22] studied the wide-area coordinated control of PSS, static SVC and auxiliary damping controller (SDC). By designing a collaborative wide-area damping controller with partial state feedback, the damping of the system damping can be improved.

Based on the aforementioned limitations, this paper aims at enhancing the stability of the system and improving the damping characteristics of the wind-PV grid-connected system by jointly using PSS, TCSC and UPFC-PODC. An improved steepest descent algorithm (SDA) is proposed to coordinate and optimize the parameters of multiple controllers. This algorithm requires less calculation than the traditional SDA and can also avoid local optimal solutions. The main contributions are as follows:

(1) Through the coordinated work of PSS and multiple FACTS devices, the LFO of the wind-PV grid-connected system is effectively suppressed, and the stability of the system is obviously improved.

(2) Proposing an improved steepest descent algorithm based on initial values optimization (ELM-SDA) to optimize the control parameters of PSS, TCSC and UPFC-PODC. Determine the initial values and value ranges of the parameters to be optimized according to the ELM to reduce the influence of the initial values error on the accuracy of the SDA, and then use the SDA to optimize the parameters to improve the overall damping characteristics of the system and enhance the dynamic stability of the system.

(3) Carrying out eigenvalue analysis and dynamic time-domain simulations to study wind-PV grid-connected system under different operating conditions, such as changing wind power and PV output, prove that the proposed ELM-SDA can be used as an effectively optimization technique to coordinate the parameters of PSS and FACTS devices.

The rest of this paper is organized as follows. Section II introduces the model of wind-PV grid-connected system, FACTS devices and PSS. Section III proposes an improved steepest descent method. Section IV uses ELM to preliminarily optimize the main parameters of PSS, TCSC and UPFC-PODC, and determine the initial values and ranges of parameters. The SDA is utilized to optimize the controller parameters. Section Ⅴ employs the eigenvalue analysis and dynamic time-domain simulation, the effectiveness of proposed ELM-SDA is fully verified through numerous results. Some useful conclusions are summarized in Section Ⅵ.

## 2. Notation

The notation used throughout the paper is stated below.

| | | | |
|---|---|---|---|
| $P_i$ | the DC winding power | $K_{\mathrm{PSS}}$ | the gain of PSS |
| $P_{ref}$ | the reference power | $T_{W1}$ | the time constant of wash-out circuit |
| $P_{\mathrm{PODC}}$ | the output power of PODC | $T_{a1}$, $T_{a2}$, $T_{a3}$ , $T_{a4}$ | the denote time constant of the lead-lag networks |
| $U_{\mathrm{UPFC}}$ | the equivalent voltage | $s^{-(k)}$ | the negative direction of the gradient |
| $T_1$, $T_2$, $T_3$, $T_4$ | the time constant of PODC | $p_k$ | the search step in the direction of the gradient |
| $K_{\mathrm{UPFC}}$ | the gain constant of UPFC | $\boldsymbol{x}$ | the vectors of the state variables |
| $T_s$, $T_a$, $T_b$ | the time constant of UPFC | $\boldsymbol{y}$ | the vectors of the algebraic variables |
| $i_c$ | the current flowing through the capacitor | $\boldsymbol{A}$ | the state matrix |
| $i_L$ | the current flowing through the inductor | $\zeta$ | the damping ratio |

| | | | |
|---|---|---|---|
| $C$ | a fixed capacitor | $\sigma_X$ | the real part of the *X-th* eigenvalue |
| $L$ | the inductor | $\zeta_X$ | the damping ratio of the *X-th* eigenvalue. |
| $U_a$ , $U_b$ | the node voltage | $\mu$ | the weighting factor |
| $I_{\mathrm{TCSC}}$ | the current flowing through the reactance | $\lambda$ | the eigenvalues of the system |
| $U_{\mathrm{TCSC}}$ | the reactance terminal voltage | $\alpha$ | the real part of the eigenvalues |
| $X_{\mathrm{TCSC}}$ | the equivalent reactance | $\beta$ | the imaginary part of the eigenvalue |
| G(s) | the transfer function of PSS | $f$ | the frequency of the oscillation |

## 3. System and controller model

### 3.1. Wind-PV grid-connected system

Through the joint development and use of wind and solar energy in time and region, it can effectively solve the problem of low utilization rate of wind power or PV power generation resources alone, realize the stability and reliability of power supply, and enhance the grid's ability to absorb intermittent renewable energy. As depicted in Figure 1, the wind-PV grid-connected system mainly includes wind power system and PV system. The wind power system is composed of doubly fed induction generator (DFIG), which is widely used. The DFIG stator is directly connected to the power system, and the rotor is connected to the system through the pulse width modulation inverter. Wind turbines convert wind energy into mechanical energy and then into electrical energy. The PV system is connected to the external power grid that can provide active and reactive power to the power system as part of the power system. The PV system usually consists of PV array, controller, inverter and power grid, among which PV array is the key part of PV system. And PV array is composed of many PV cells connected in series or in parallel. Each PV cell is formed of a PN-type semiconductor, which can generate electric current through the photovoltaic effect.

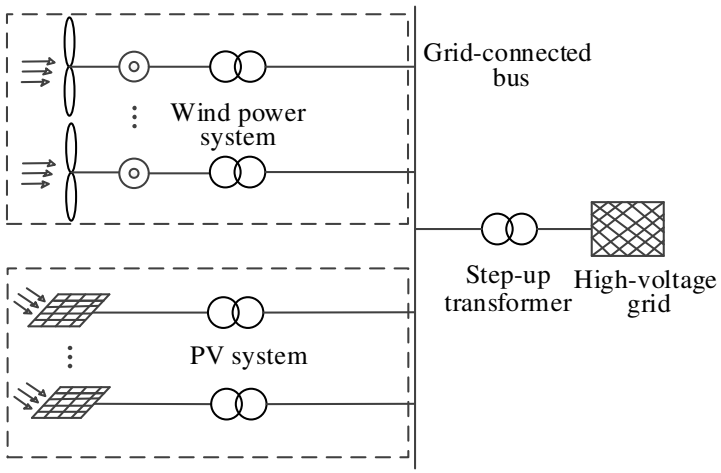

**Figure 1** The structure diagram of wind-PV grid-connected system

3.2. The model of UPFC-PODC

When the power system encounters low frequency oscillation, it may cause large-scale power oscillations and undermine the stability of the system. The amplitude of system oscillation is closely related to its own damping level. By improving the damping characteristics of the system, low frequency oscillation can be effectively suppressed and the stability of the system can be enhanced. If the system itself is insufficiently damped and additional damping is required, PODC is considered to increase the overall damping level of the system and suppress system oscillation. The structure of PODC based on UPFC is shown in Figure 2.

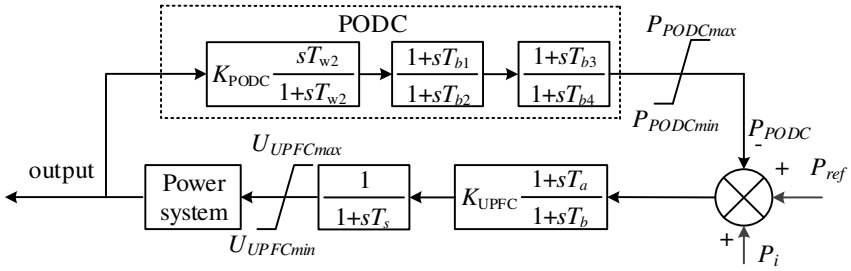


**Figure 2** The structure diagram of UPFC-PODC

where $P_i$ is the DC winding power; $P_{ref}$ is the reference power; $P_{PODC}$ is the output power of PODC; $U_{UPFC}$ is the equivalent voltage; $T_1$, $T_2$, $T_3$, $T_4$ are the time constant of PODC; $K_{UPFC}$, $T_s$, $T_a$, $T_b$ are the gain and time constant of UPFC.

3.3. The model of TCSC

The structure of TCSC is shown in Figure 3. The main circuit is composed of capacitors, bypass inductors, anti-parallel controllable thyristors and zinc oxide arresters. TCSC changes the current flowing through the reactor by controlling the firing angle α of the thyristor [13], thereby changing the line impedance value and continuously controlling the line power.

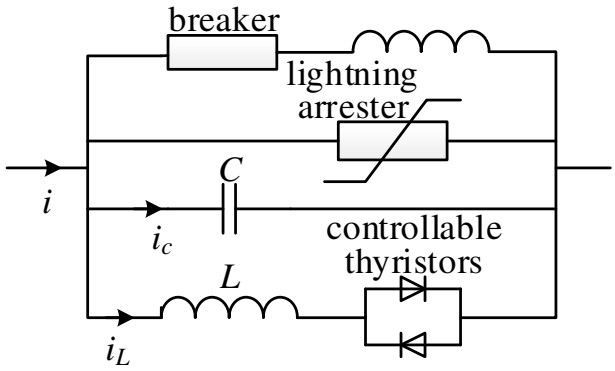


**Figure 3** The structure diagram of TCSC.

where $i_c$ is the current flowing through the capacitor; $i_L$ is the current flowing through the inductor; $C$ is a fixed capacitor; $L$ is the inductor.
To facilitate calculation, TCSC can be regarded as a variable reactance connected in series in the line. The steady-state circuit of TCSC is shown in Figure 4, which can be obtained:

$$U_{\mathrm{TCSC}} = -I_{\mathrm{TCSC}} \cdot \mathrm{j}X_{\mathrm{TCSC}} \tag{1}$$

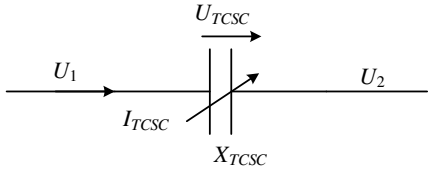


**Figure 4** Steady state circuit diagram of TCSC.

where $U_a$ and $U_b$ are the node voltage; $I_{TCSC}$ is the current flowing through the reactance; $U_{TCSC}$ is the reactance terminal voltage; $X_{TCSC}$ is the equivalent reactance.

3.4. The model of PSS

Power system stabilizer (PSS) is an additional excitation control technology that is researched to suppress low-frequency oscillation. It introduces an additional signal ahead of the shaft speed in the excitation voltage regulator to generate a positive damping torque to overcome the negative damping torque generated in the original excitation voltage regulator [8]. PSS is used to improve the damping of the power system and solve the problem of low frequency oscillation. It is one of the important measures to improve the dynamic stability of the power system.
It extracts signals related to this oscillation, such as generator active power, speed or frequency, and processes them. The additional signals generated are added to the excitation regulator to make the generator generate additional torque that dampens low frequency oscillations. The transfer function $G(\mathrm{s})$ can be expressed as:

$$G(\mathrm{s}) = K_{\mathrm{PSS}} \frac{sT_{W1}}{1+sT_{W1}} \frac{1+sT_{a1}}{1+sT_{a2}} \frac{1+sT_{a3}}{1+sT_{a4}} \tag{2}$$

where $K_{\mathrm{PSS}}$ is the gain of PSS; $T_{W1}$ is the time constant of wash-out circuit; $T_{a1}$, $T_{a2}$, $T_{a3}$ and $T_{a4}$ denote time constant of the lead-lag networks.

## 4. Proposed improved steepest descent algorithm

4.1. Application of the steepest descent algorithm and its shortcomings

The steepest descent algorithm (SDA) is one of the classic algorithm used to solve parameter optimization problems [23]. It uses the negative gradient direction as the search direction, because the negative gradient direction is the fastest descending direction of the function, so the next point searched in this direction must be better than the original, and there are no meaningless iteration situations, so SDA can find the minimum effectively. Its iterative formula is shown in Eq. (3).

$$a_{k+1} = a_k + p_k s^{-(k)} \tag{3}$$

where $s^{-(k)}$ represents the negative direction of the gradient, $p_k$ represents the search step in the direction of the gradient.

The gradient direction can be obtained by deriving the function. The determination of the step length is more troublesome. If it is too large, it may diverge, and if it is too small, the convergence speed is too slow. Generally, the method of determining the step size is determined by the linear search algorithm, that is, the coordinate of the next point is regarded as a function of $a_{k+1}$, and then $a_{k+1}$ that satisfies the minimum value of $f(a_{k+1})$ can be obtained. When the traditional SDA is used for optimization, the termination condition of the algorithm iteration is that the magnitude of the gradient vector is close to 0, and a very small constant threshold can be set. Since the steepest descent method is based on the idea of Newton's method, and Newton's method has strict requirements on the initial value of the iteration, the initial value has a relatively large impact on SDA, and improper selection of the initial value may cause the function to not converge and the extreme value cannot be obtained.

In summary, in order to make full use of the advantages of SDA's simple principle and fast convergence speed, the calculation efficiency can be improved by selecting appropriate initial values, and it can also avoid SDA from falling into a local optimal solution.

### 4.2. A method of steepest descent algorithm based on eigenvalue locus movement

The state space representation of the power system can be written as a differential algebraic equation, as shown in Eq. (4)

$$\begin{cases} \dot{\boldsymbol{x}} = f(\boldsymbol{x}, \boldsymbol{y}) \\ 0 = g(\boldsymbol{x}, \boldsymbol{y}) \end{cases} \tag{4}$$

where $\boldsymbol{x}$ and $\boldsymbol{y}$ are the vectors of the state variables and the algebraic variables, respectively. Based on the linear system and Lyapunov theory, eigenvalue analysis is the most appropriate method to study the small signal stability of the power system. The linearized model (5) is obtained from the Taylor series expansion at the system stable operating point ($x_s$, $y_s$).

$$\begin{bmatrix} \Delta\dot{\boldsymbol{x}} \\ 0 \end{bmatrix} = \begin{bmatrix} \nabla_x f & \nabla_y f \\ \nabla_x g & \nabla_y g \end{bmatrix} \begin{bmatrix} \Delta\boldsymbol{x} \\ \Delta\boldsymbol{y} \end{bmatrix} = \begin{bmatrix} \boldsymbol{A}_1 & \boldsymbol{B}_1 \\ \boldsymbol{C}_1 & \boldsymbol{D}_1 \end{bmatrix} \begin{bmatrix} \Delta\boldsymbol{x} \\ \Delta\boldsymbol{y} \end{bmatrix} \tag{5}$$

where $\nabla_x f$ is the gradient of the function $f(\boldsymbol{x}, \boldsymbol{y})$, and $\nabla_x f = \partial f(\boldsymbol{x}, \boldsymbol{y}) / \partial \boldsymbol{x}$, other remaining similar symbols have similar definitions. By considering $\nabla_x g$ is non-singular, then (5) can be written as

$$\Delta\dot{\boldsymbol{x}} = \left[ \boldsymbol{A}_1 - \boldsymbol{B}_1 (\boldsymbol{C}_1)^{-1} \boldsymbol{D}_1 \right] \Delta\boldsymbol{x} = \boldsymbol{A}\Delta\boldsymbol{x} \tag{6}$$

where A is the state matrix. After that, the stability of the system could be analysed by calculations on the eigenvalues of matrix A. The complex eigenvalues of matrix A are $\lambda = \alpha \pm j\beta$, $f = \beta / 2\pi$ is the oscillation frequency, the damping ratio is defined as

$$\zeta(\%) = \frac{-\alpha}{\sqrt{\alpha^2 + \beta^2}} \times 100\% \tag{7}$$

When the eigenvalues of the characteristic equation change in a certain range with a certain parameter of the controller, the locus formed on the complex plane is called the eigenvalue locus. The method used as a diagram can represents the entire numerical relationship between the eigenvalues of the characteristic equation and a certain parameter of the system. When this parameter takes a specific value, the corresponding eigenvalues can be found in the above relationship graph. This method is called eigenvalue locus method (ELM) and has intuitive advantages. The eigenvalue locus of the system can be used to analyse the stability and transient response characteristics of the system with known structure and parameters, and it can also analyse the impact of parameter changes on system performance. In the small-signal stability analysis of power system, it is of great

significance to study the distribution of eigenvalues on the complex axis. If the real parts of all eigenvalues of the state matrix are negative, the system is stable under small disturbance; if at least one of the real parts of all eigenvalues is positive, the system is unstable under small disturbance; if all eigenvalues have no real part that is positive, but at least one real part is zero, then the system is critically stable.

In this paper, the author proposes an improved SDA based on initial value optimization, while coordinating the control parameters of PSS, TCSC and UPFC-PODC to improve the damping characteristics of the wind and solar grid-connected system and enhance the stability of the system. In order to solve the high sensitivity of the SDA to the initial value, first, through the eigenvalue calculation, the eigenvalues closely related to the low frequency oscillation mode of the system are obtained. Then, use the ELM to draw the change trend graph corresponding to these key eigenvalues on the complex plane. If the eigenvalue change trend meets the requirements, the value range is continuously reduced to approach the optimal range until a suitable initial value of the SDA is found. If it does not meet the requirements, reselect the initial value and repeat the above steps. Finally, the steepest descent algorithm based on the initial value optimization is used to coordinate and optimize the parameters between different controllers, so that the system eigenvalues move to the negative half axis of the virtual axis as much as possible, until the damping level of the system meets the expected requirements.

## 5. Parameters optimization of multiple damping cotrollers

### 5.1. Classic example system

In this section, the Western System Coordinating Council (WSCC) eight machines twenty-four buses system is chosen as the study system, which includes eight synchronous generators (SG) and nine load buses as shown in Figure 5. Here, the SG is uniformly represented by sixth-order model and the base capacity of SG is set to 100 MVA. The system frequency is 50 Hz and the other detailed parameters can be found in [24]. For the convenience of analysis, this paper uses wind turbines and photovoltaic (PV) stand-alone models to replace the lumped models of wind farms and PV stations. The wind farm is connected to the system via bus 4, and the wind turbine output is 60 MW. The PV station is connected to the system via bus 9, and the PV output is 50 MW. Each SG is equipped with PSS. With the help of the residue index of the open-loop system [25], consider connecting TCSC between bus 6 and bus 7, and connecting UPFC-PODC between bus 7 and bus 16.

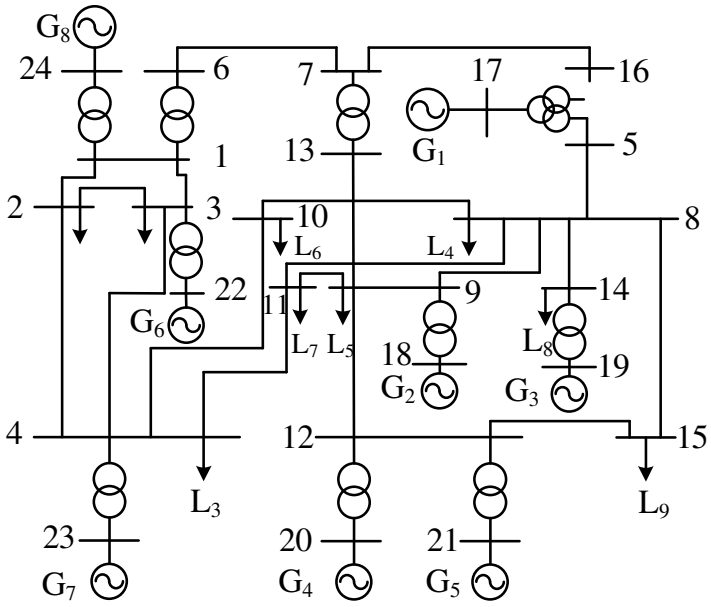


**Figure 5** The WSCC eight machines twenty-four buses system

The power system composed of N machines has N-1 electromechanical oscillation modes. According to the modal analysis of the eigenvalues, there are seven oscillation modes in the above power system. Through the eigenvalues calculation, Table 1 gives partial eigenvalues calculation results of the study system without PSS and FACTS devices, including damping ratio, oscillation frequency and dominant machines (DM).

**Table 1** Partial eigenvalue calculation results of the system

| Mode | $\lambda$ | $\zeta$(%) | $f$(Hz) | DM |
|---|---|---|---|---|
| 1 | -2.0807±j16.9267 | 12.20 | 2.8870 | G1,G3 |
| 2 | -1.3351±j12.8188 | 10.36 | 2.0277 | G2,G6 |
| 3 | -0.9255±j12.5165 | 7.37 | 1.8164 | G3,G5 |
| 4 | -0.8381±j10.2740 | 8.13 | 1.6407 | G4,G5 |
| 5 | -0.8279±j8.5743 | 9.61 | 1.3690 | G5,G7 |
| 6 | -0.5760±j7.1235 | 8.06 | 1.1374 | G7,G8 |
| 7 | -0.0370±j4.1589 | 0.90 | 0.6601 | G6,G7 |

After the wind farm and PV station are connected to the power system, due to their uncertainty and intermittency, they are bound to have a certain impact on the dynamic stability of the system, especially the small signal stability of the system. TCSC can change the impedance value of the line according to the change of the control signal, such as line power, so as to control the power flow distribution in the power system. When TCSC is used for power modulation, the compensation degree of TCSC can be controlled according to the selected auxiliary signal, and the transmission power of the transmission line can be changed, thereby suppressing the low frequency oscillation of the power system. The amplitude of the power system power oscillation is closely related to the system damping level. Increasing the system damping can reduce the power oscillation amplitude. The addition of the UPFC-PODC optimizes the system damping characteristics, thereby enhancing the small signal stability of the system. Table 2 shows the calculation results of

the electromechanical oscillation modes of the power system with PSS, TCSC and UPFC-PODC simultaneously.

**Table 2** Partial eigenvalues results of the system after installing PSS, TCSC and UPFC-PODC

| Mode | $\lambda$ | $\zeta$(%) | $f$(Hz) | DM |
|---|---|---|---|---|
| 1 | -2.8325±j18.2760 | 15.32 | 2.9434 | G1,G3 |
| 2 | -1.3311±j12.7729 | 10.37 | 2.0439 | G2,G6 |
| 3 | -0.9358±j11.3335 | 8.23 | 1.8098 | G3,G5 |
| 4 | -0.868±j10.2748 | 8.12 | 1.6457 | G4,G5 |
| 5 | -0.8314±j9.5613 | 8.66 | 1.3647 | G5,G7 |
| 6 | -0.5310±j7.1614 | 7.39 | 1.1403 | G7,G8 |
| 7 | -0.0394±j4.1472 | 0.95 | 0.6647 | G6,G7 |

Comparing Table 1 and Table 2, it can be found that after installing PSS, TCSC and UPFC-PODC, the damping ratios of some oscillation modes of the system have been improved to a certain extent. However, this degree of improvement has a very limited effect on enhancing system stability and cannot reach a satisfactory level. And the damping $\lambda_7$ is too small, which is not conducive to system stability. Therefore, in order to improve the small signal stability of the wind-PV grid-connected system, an improved steepest descent algorithm ELM-SDA is proposed to coordinate and optimize the control parameters of FACTS devices and PSSs, so that the key eigenvalues of the system can be far away from the virtual axis and improve the overall damping level of the system to enhance the stability of the system.

5.2. Optimization of parameters initial values based on ELM

Appropriate initial values can greatly improve the operation efficiency of SDA, and can also prevent SDA from falling into the local optimal solution. The parameters to be optimized in this paper are the gain of PSS ($K_{PSS}$), the gain of TCSC ($K_{TCSC}$) and the gain of UPFC-PODC ($K_{PODC}$). In this section, the ELM is employed to select a set of optimal parameters as the initial value of subsequent optimization, and to determine the value range of each parameter at the same time. When two of these parameters are fixed and the other parameter changes within a certain range, the eigenvalues of the system will change accordingly, and the change law will form a trajectory, which is the eigenvalue locus of the system. According to the change trend of the eigenvalue locus, an appropriate value can be selected as the initial value. Here, appropriate means that the critical eigenvalues of the system can be moved away from the imaginary axis to increase the anti-interference ability of the system.

First, randomly generate three integers within the value range of the above controller [1, 100], and assign them to $K_{PSS}$, $K_{TCSC}$ and $K_{PODC}$ respectively. Then fix the values of $K_{PSS}$ and $K_{TCSC}$, make $K_{PODC}$ change in the range of [1, 100], and finally draw the eigenvalues locus movement diagrams of the system according to the change of the eigenvalues. The corresponding locus movement diagrams of some critical eigenvalues of the system are shown in Figure 6.

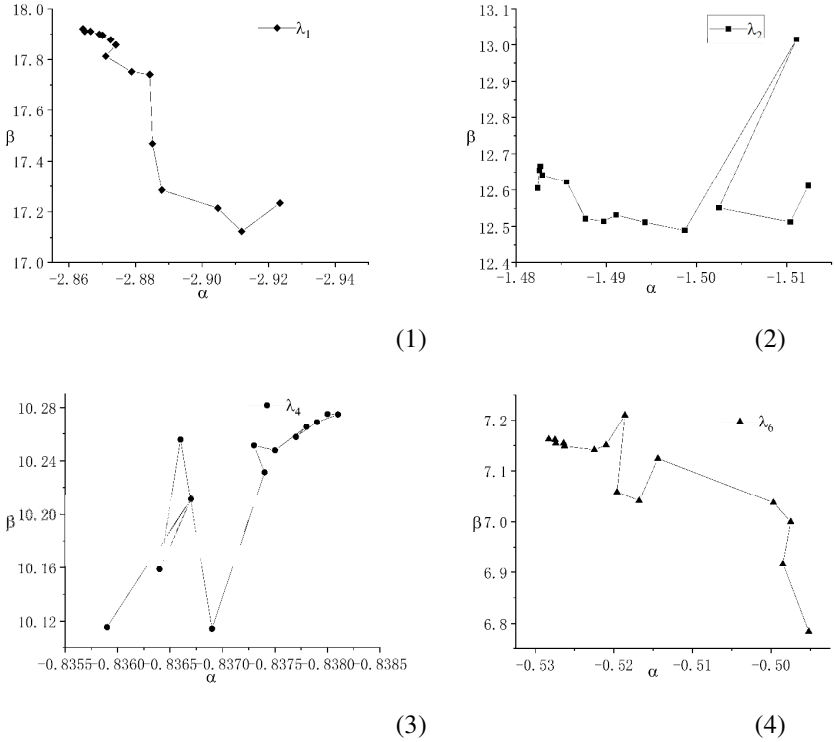


**Figure 6** The ELM diagrams of system when $K_{PODC}$ changes :

As can be seen from Fig. 8 that with the change of $K_{PODC}$, $\lambda_1$ is initially away from the imaginary axis and continues to move away from the imaginary axis, $\lambda_2$ also gradually away from the imaginary axis, the variation of $\lambda_4$ is not obvious and $\lambda_6$ tends to approach the imaginary axis.

Because $\lambda_7$ not only corresponds to the low frequency oscillation of the power system, but its damping ratio is also relatively small. Therefore, before determining the optimal initial values of PSS, TCSC and UPFC-PODC, it is important for us to first consider increasing its damping ratio and keeping other critical eigenvalues far away from the imaginary axis. At the same time, it cannot be ignored that when $K_{PODC}$ changes, $\lambda_6$ tends to become a positive value, which is not conducive to the stability of the small signal of the system. With reference to the variation trend of the key eigenvalues of the system, the initial optimization value of $K_{PODC}$ is determined to be 10 and its value range is [5, 50]. Similarly, $K_{PSS}$ and $K_{TCSC}$ can be determined by applying the above optimization scheme. The initial value of $K_{PSS}$ is 15 and its value range is [10, 60]. The initial value of $K_{TCSC}$ is 5 and its value range is [1,40],

In this way, the parameter initial values and value ranges for preliminary optimization using the ELM are obtained. Since the optimization process has not been rigorous, the accuracy of the damping controller parameters is not very high. Therefore, SDA will be employed to further optimize the parameters in the next stage to improve the damping characteristics of the system and enhance the dynamic stability of the system.

5.3. Optimization of parameters based on SDA

The basic idea of SDA is to use the negative gradient direction as the search direction, because the negative gradient direction is the fastest descending direction of the function, the next point searched in the negative gradient direction must be better than the original, and it will not appear meaningless iteration situation, so the SDA can effectively find the minimum of the problem [23]. The advantage of the SDA is that the algorithm is simple and has better search ability. However, if it starts from the wrong point, it will perform numerous iterations, and may also converge to the local minimum. Thus, in this section, the multiple gain parameters obtained by ELM in the previous section are used as the initial values of SDA to avoid the algorithm from falling into the local optimal solution and improve the efficiency of SDA.

In order to coordinate the PSS, TCSC and UPFC-PODC installed in the system simultaneously, to improve the overall damping level of the system, an appropriate objective function is designed, which is an expression that employs the optimized parameters as inputs variables to describe the mathematical relationship of the optimized parameters. The objective function $F(X)$ is described as:

$$F(X)=\sum_{\sigma_0\geq\sigma_X}(\sigma_0\text{-}\sigma_X)^2+\mu\sum_{\zeta_X\geq\zeta_0}(\zeta_0\text{-}\zeta_X)^2 \tag{8}$$

where $\sigma_X$ is the real part of the *X-th* eigenvalue that has the most influence on system stability, $\zeta_X$ represents the damping ratio of the *X-th* eigenvalue. $\mu$ is the weighting factor selected from the experience of reference, which is used to solve the stability enhancement problems of multi-objective power systems, with the purpose of keeping two parts of $F(X)$ in the same order of magnitude.

Therefore, the problem of controller parameters optimization can be transformed into a problem of finding the extreme value of the objective function, that is, minimizing $F(X)$. Moreover, the values of $K_{PSS}$, $K_{TCSC}$ and $K_{PODC}$ are subject to the range of parameters obtained using ELM, and the value ranges of the above gains are:

$$\begin{aligned} 10 &\leq K_{PSS} \leq 60 \\ 1 &\leq K_{TCSC} \leq 40 \\ 5 &\leq K_{PODC} \leq 50 \end{aligned} \tag{9}$$

The optimization process of SDA is as follows:

Step1: Take the initial optimization parameter as $X^{(1)}$, the number of iterations $i = 1$, set the initial value of the matrix $\boldsymbol{H} = \mathbf{[1]}$, the maximum number of iterations is $i_{max}$.

Step2: Calculate the gradient $\nabla F(X^{(i)})$ of the objective function $F(X)$,

$\nabla F(X^{(i)})=\partial F(X)/\partial X]_{X=X^{(i)}}$.

Step3: Define direction $S^{(i)}=-H^{(i)}\nabla F(X^{(i)})$, use the one-dimensional search method in direction $S^{(i)}$ to get the best step $\mu^{(i)}$, satisfy the iteration formula:

$$X^{(i+1)}=X^{(i)}-\mu^{(i)}\boldsymbol{H}^{(i)}\nabla F(X^{(i)}) \tag{10}$$

Step4: Apply the optimization parameter $X^{(i+1)}$ as the variable of the objective function $F(X)$. If $F(X)$ achieves the minimum value, then $X^{(i+1)}$ is the optimal solution, and the iteration ends, otherwise, go to step 5.

Step5: Calculate the gradient $\nabla F(X^{(i+1)})$ of the objective function $F(X)$ at the parameter $X^{(i+1)}$, make $\nabla G^{(i)}=\nabla F(X^{(i+1)})- \nabla F(X^{(i)})$.

Step6: Improve matrix H(i+1), let

$$\boldsymbol{H}^{(i+1)}=\boldsymbol{H}^{(i)}+\frac{\Delta X^{(i)}\Delta X^{(i)^T}}{\Delta X^{(i)^T}\Delta G^{(i)}}+\frac{(\boldsymbol{H}^{(i)}\Delta G^{(i)})(\boldsymbol{H}^{(i)}\Delta G^{(i)})^T}{\Delta G^{(i)^T}\boldsymbol{H}^{(i)}\Delta G^{(i)}} \tag{11}$$

Step7: The number of iterations $i = i+1$, if $i < i_{max}$, return to Step 3, otherwise, end the iteration process and output the optimization parameter of the last iteration.

## 6. Simulation results

In this section, the proposed improved algorithm ELM-SDA has been used to search for the optimal settings of PSS, TCSC the effectiveness of ELM-SDA in improving the damping characteristics of the system, the small disturbance eigenvalue analysis has been carried out and compared with SDA. The calculation results of the system eigenvalues analysis are shown in Table 3.

**Table 3** Partial eigenvalue calculation results under different algorithms

| | Algorithm : SDA | | | algorithm :ELM-SDA | | | |
|---|---|---|---|---|---|---|---|
| M | λ | ζ(%) | *f*(Hz) | λ | ζ(%) | *f*(Hz) | DM |
| 1 | -3.7859±j15.4843 | 24.19 | 2.8874 | -4.7631±j14.2874 | 31.62 | 2.9124 | G1,G3 |
| 2 | -1.9873±j11.5482 | 16.96 | 2.0437 | -2.3215±j10.7579 | 21.09 | 2.0413 | G2,G6 |
| 3 | -1.0895±j10.1711 | 10.65 | 1.8018 | -1.5517±j9.7028 | 15.79 | 1.8122 | G3,G5 |
| 4 | -0.9813±j10.5482 | 9.26 | 1.6488 | -1.2959±j10.7411 | 11.98 | 1.6510 | G5,G7 |
| 5 | -0.9541±j10.2118 | 9.30 | 1.3713 | -0.9685±j8.8742 | 10.85 | 1.3710 | G4,G5 |
| 6 | -0.5997±j6.9854 | 8.55 | 1.1431 | -0.8819±j8.9587 | 9.80 | 1.1434 | G7,G8 |
| 7 | -0.1569±j5.8547 | 2.68 | 0.6617 | -0.2127±j4.7451 | 4.36 | 0.6642 | G6,G7 |

It can be seen from Table 3 that the proposed ELM-SDA effectively improves the critical eigenvalues related to the low frequency oscillation modes of the system, and the corresponding damping ratios have also been significantly improved. Compared with the classic SDA, the damping characteristics of the system are further improved. Among them, the eigenvalues and damping ratios of oscillation modes 1, 2 and 3 have the greatest degree of improvement, the eigenvalues of modes 4, 5 and 6 have been improved to a certain extent, and the weak eigenvalue λ7 corresponding to oscillation mode 7 has also been effectively improved, which is conducive to enhancing system stability. It shows that the overall damping level of the system has been improved, and the small signal stability of the system has also been effectively enhanced.

In order to further verify the effectiveness of the proposed ELM-SDA in parameters coordination and optimization, the dynamic time-domain simulation of the system has been carried out next. Assume that there is a three-phase short-circuit fault occurs in between bus 8 and bus 9 at the fault time ts=1.0s, the fault clearing time is 0.05s, and the power system is put back into operation at 1.05s. The response curves of system power angle and active power under fault are shown in Figure 7.

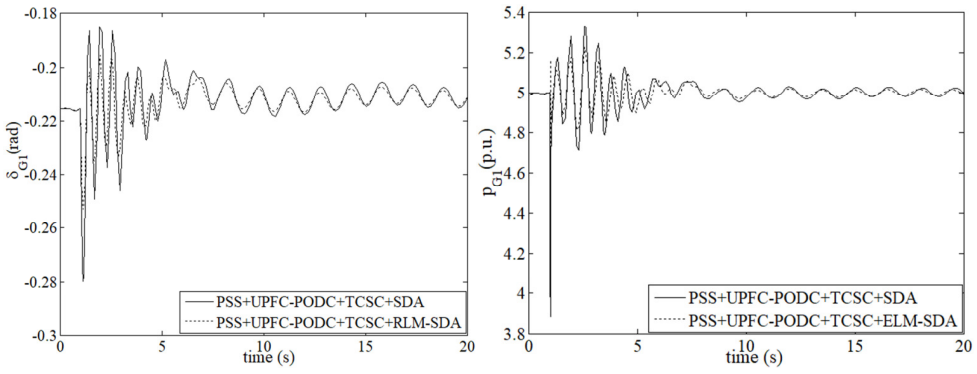


**Figure 7** $\delta$ and P response curves of the system

It can be seen from Figure 7 that after parameter optimization using ELM-SDA, compared with the traditional SDA, when the system encounters a three-phase short-circuit fault, the system power angle and active power oscillation amplitude are significantly reduced, and the time required for the system to recover stability also drastically reduced. This shows that the system has a better damping effect on low frequency oscillation and improves stability of the system. The simulation results also proved the superiority of the proposed ELM-SDA in the coordination and optimization of controller parameters.

6.1. System simulation of wind power and PV output changes

In the case of changing the output of wind power and PV respectively, the influence of PSS, TCSC and UPFC-PODC on the stability of the system after parameters optimization using ELM-SDA is studied. Table 4 shows the comparison of systems that increase the wind power and PV output by 10% and 30%, respectively.

**Table 4** Partial eigenvalue calculation results after parameters optimization.

| Output | | Both increase | | 10% | Both increase | | 30% | |
|---|---|---|---|---|---|---|---|---|
| | M | λ | ζ(%) | *f*(Hz) | λ | ζ(%) | *f*(Hz) | DM |
| Before Optimizatio | 1 | -2.7959±j18.3127 | 15.09 | 2.9145 | -2.5717±j18.0674 | 14.09 | 2.9096 | G1,G3 |
| | 2 | -1.3278±j12.8106 | 10.31 | 2.0498 | -1.3054±j12.8216 | 10.13 | 2.0517 | G2,G6 |
| | 3 | -0.9661±j11.3428 | 8.49 | 1.8113 | -0.9305±j11.6725 | 7.95 | 1.8165 | G3,G5 |
| | 4 | -0.8362±j8.5737 | 9.71 | 1.6496 | -0.8281±j9.1727 | 8.99 | 1.6402 | G5,G7 |
| | 5 | -0.8279±j10.3330 | 7.99 | 1.3709 | -0.8144±j10.4301 | 7.78 | 1.3711 | G4,G5 |
| | 6 | -0.5305±j7.1620 | 7.39 | 1.1431 | -0.5254±j7.8869 | 6.65 | 1.1426 | G7,G8 |
| | 7 | -0.0377±j4.1662 | 0.90 | 0.6631 | -0.0358±j4.1378 | 0.87 | 0.6587 | G6,G7 |
| After Optimization | 1 | -3.7971±j16.1733 | 22.86 | 2.9491 | -3.7897±j16.0215 | 23.02 | 2.9024 | G1,G3 |
| | 2 | -2.5221±j12.7631 | 19.39 | 2.0422 | -2.3298±j11.0477 | 20.63 | 2.0443 | G2,G6 |
| | 3 | -1.3471±j9.3419 | 14.27 | 1.8111 | -1.2875±j8.8712 | 14.36 | 1.816 | G3,G5 |
| | 4 | -0.9238±j8.3331 | 11.02 | 1.6497 | -0.9306±j8.6396 | 10.83 | 1.6403 | G5,G7 |
| | 5 | -0.9041±j9.1753 | 9.81 | 1.3709 | -0.9262±j10.3349 | 8.93 | 1.3685 | G4,G5 |
| | 6 | -0.6692±j7.2559 | 9.18 | 1.1430 | -0.6073±j7.1572 | 8.45 | 1.1417 | G7,G8 |
| | 7 | -0.1568±j3.1680 | 4.94 | 0.6633 | -0.1554±j4.1385 | 3.75 | 0.6587 | G6,G7 |

It can be observed from Table 4 that after the controller parameters optimization, when the output of wind and PV power both increase, the critical eigenvalues and damping ratios of the system have been all enhanced. Especially when the wind and PV power output both increased by 30%, not only will the eigenvalues improvement effect of system oscillation modes 1, 2 and 3 be better, the overall damping characteristics of the system will also be effectively improved.

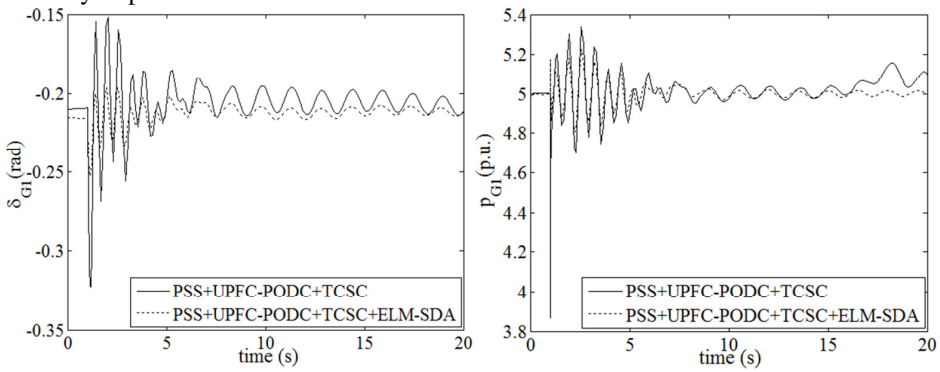


**Figure 8** δ and P response curves after wind and PV power output increase by 10%

Under the conditions of increasing the wind and PV power output, the performance of the proposed ELM-SDA under system three-phase short-circuit fault is verified. Figure 8 and Figure 9 show the system response curves after increasing the wind and PV power output, respectively.

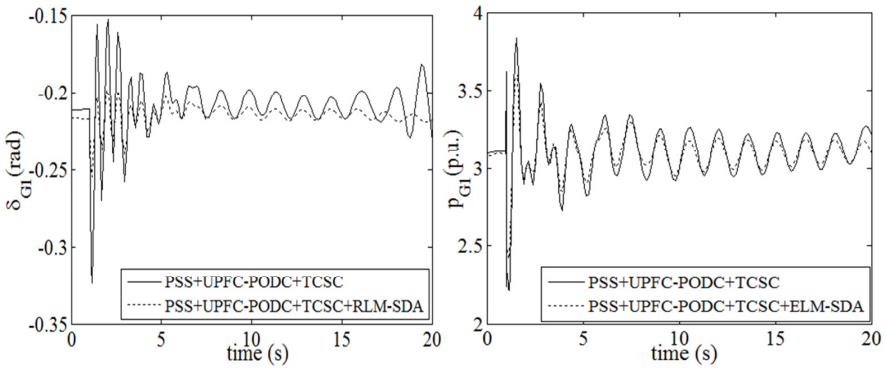


**Figure 9** δ and P response curves after wind and PV power output increase by 30%

As shown in Figure 8 and Figure 9, we can find that under the premise of increasing output of wind and PV power, when the system encounters the short-circuit fault, the power angle and active power of system will experience severe and continuous oscillations, and it takes a long time to restore stability. At this moment, by employing the proposed ELM-SDA to optimize the controller parameters, it can be clearly seen that the power angle and active power amplitudes are significantly reduced when a fault is encountered, and the stabilization time is also shortened. In addition, when the output of wind and PV power both increased by 30%, the system oscillations will be more serious. Through parameters optimization, the system will quickly stabilize after undergoing a brief small oscillation after the fault, which also confirms the effectiveness of the proposed algorithm ELM-SDA in suppressing low frequency oscillation of the system and improving the stability of the system.

6.2. System simulation of WF and PV station access point changes

This section studies the impact of changing WF and PV station access points on the system stability. The effectiveness of the proposed algorithm ELM-SDA is verified by the following two calculation examples. Case 1: Connect the WF at bus 9 and the PV station at bus 4. Case 2: Connect the WF at bus 12 and the PV station at bus 14.

Table 5 summarizes partial eigenvalues of the system that change the access points of WF and PV station. From Table 5, after parameters optimization, when the access points of WF and PV station in the system change, the weak eigenvalues and damping ratios of the system have been enhanced to a certain extent, while the largest eigenvalues $\lambda_7$ has been also improved. This also shows that the small signal stability of the system has been strengthened.

**Table 5** Partial eigenvalue calculation results after parameters optimization.

| Case | | Case1 | | | Case2 | | | |
|---|---|---|---|---|---|---|---|---|
| | M | λ | ζ(%) | *f*(Hz) | λ | ζ(%) | *f*(Hz) | DM |
| Before Optim ization | 1 | -2.8641±j18.9117 | 14.98 | 2.8870 | -2.4811±j17.3983 | 14.12 | 2.8193 | G1,G3 |
| | 2 | -1.3822±j12.8847 | 10.67 | 2.0157 | -1.3379±j12.5844 | 10.57 | 2.0142 | G2,G6 |
| | 3 | -0.9675±j11.3715 | 8.48 | 1.8098 | -0.9381±j11.1178 | 8.41 | 1.7749 | G3,G5 |
| | 4 | -0.8368±j8.8716 | 9.39 | 1.6407 | -0.8761±j10.1871 | 8.57 | 1.6266 | G5,G7 |
| | 5 | -0.8314±j8.5613 | 9.67 | 1.3690 | -0.8324±j10.3701 | 8.00 | 1.3681 | G4,G5 |
| | 6 | -0.5561±j7.2615 | 7.64 | 1.1374 | -0.5281±j7.1217 | 7.40 | 1.1374 | G7,G8 |
| | 7 | -0.0394±j4.1472 | 0.95 | 0.6601 | -0.0407±j4.1156 | 0.99 | 0.6551 | G6,G7 |
| After Optimi zation | 1 | -3.9022±j16.3728 | 23.18 | 2.9009 | -3.8143±j15.1097 | 24.48 | 2.6841 | G1,G3 |
| | 2 | -2.6753±j12.1365 | 21.52 | 2.0438 | -2.3024±j12.3683 | 18.31 | 2.0302 | G2,G6 |
| | 3 | -1.3295±j9.7183 | 13.55 | 1.8164 | -1.3041±j8.5874 | 15.01 | 1.7835 | G3,G5 |
| | 4 | -0.9283±j8.3551 | 11.04 | 1.6407 | -0.9344±j8.5696 | 10.84 | 1.6268 | G5,G7 |
| | 5 | -0.9147±j9.1744 | 9.92 | 1.3136 | -0.9415±j10.1821 | 9.21 | 1.3297 | G4,G5 |
| | 6 | -0.6672±j7.3727 | 9.01 | 1.3429 | -0.6431±j7.1690 | 8.93 | 1.3434 | G7,G8 |
| | 7 | -0.1396±j3.5689 | 3.91 | 0.6620 | -0.1359±j4.1279 | 3.29 | 0.6570 | G6,G7 |

Similarly, when the system encounters the three-phase short-circuit fault, we will verify the performance of the proposed ELM-SDA in the time-domain simulation. Figure 10 and Figure 11 show the dynamic time-domain simulation results of changing the access points of WF and PV station.

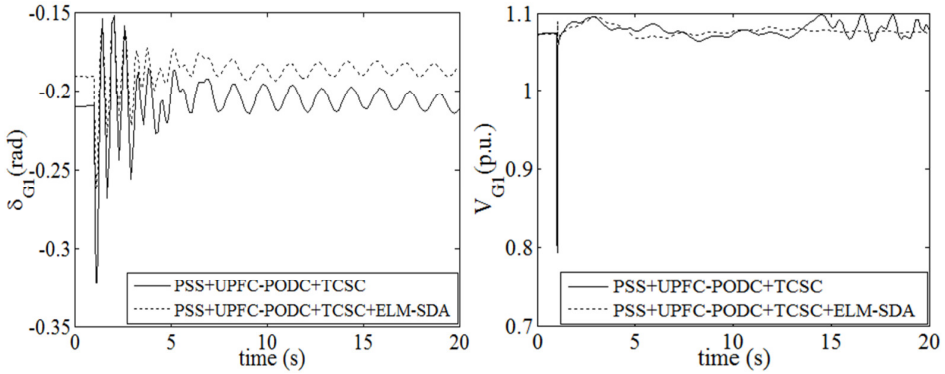


**Figure 10** δ and V response curves of Case 1

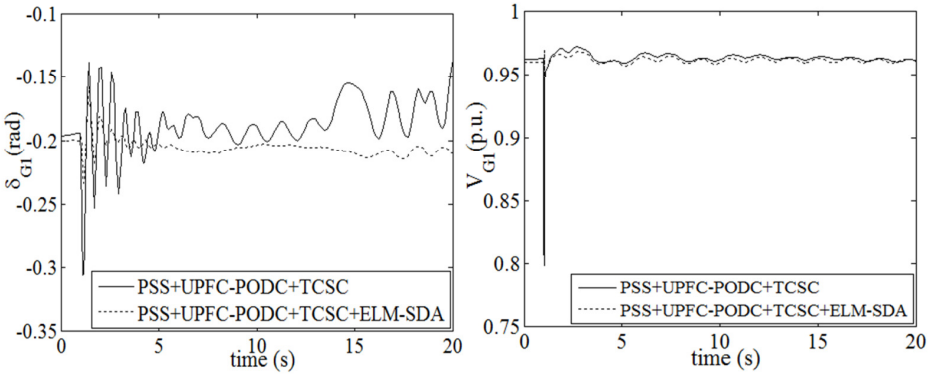


**Figure 11** δ and V response curves of Case 2

It is obviously that the access point of the WF and PV station in the system is changed, the feature of system oscillation curves is different. When the WF and PV station are switched in positions, the power angle of the generator 1 experiences stronger oscillations and takes more time to restore stability, and when they change the positions again, the voltage oscillation amplitude is relatively small, and the oscillation duration is short. After parameter optimization, the system power angle and voltage oscillation amplitudes are significantly reduced, and the time to regain stability has also been greatly shortened.

6.3. System simulation of UPFC-PODC compensation changes

In this section, through the eigenvalue analysis method and dynamic time-domain simulation, the impact of UPFC-PODC with different series compensation percentages (CP) on the dynamic stability of the system is examined. The performance of the proposed ELM-SDA is verified by the following two examples. Case 3: Increase CP to 35%, Case 4: Decrease CP to 10%. The comparison of system partial oscillation modes is shown in Table 6.

**Table 6** Partial eigenvalue calculation results after parameters optimization

| Case | | Case3 | | | Case4 | | | |
|---|---|---|---|---|---|---|---|---|
| | M | λ | ζ(%) | *f*(Hz) | λ | ζ(%) | *f*(Hz) | DM |
| Before Optimization | 1 | -2.8210±j18.2863 | 15.25 | 2.9448 | -2.8641±j17.9117 | 15.79 | 2.9116 | G1,G3 |
| | 2 | -1.3281±j12.7901 | 10.33 | 2.0466 | -1.4822±j12.6653 | 11.62 | 2.0376 | G2,G6 |
| | 3 | -0.9277±j11.3419 | 8.15 | 1.8112 | -0.9675±j11.3715 | 8.48 | 1.8062 | G3,G5 |
| | 4 | -0.8297±j8.5641 | 9.64 | 1.6513 | -0.8491±j9.3469 | 9.05 | 1.6519 | G5,G7 |
| | 5 | -0.8203±j10.3430 | 7.91 | 1.363 | -0.8319±j10.4161 | 7.96 | 1.3674 | G4,G5 |
| | 6 | -0.5329±j7.1751 | 7.41 | 1.1451 | -0.5418±j7.1907 | 7.51 | 1.1477 | G7,G8 |
| | 7 | -0.0386±j4.1816 | 0.92 | 0.6655 | -0.0452±j4.1891 | 1.08 | 0.6674 | G6,G7 |
| After Optimization | 1 | -3.6323±j17.0183 | 20.87 | 2.9456 | -3.8315±j16.2805 | 22.91 | 2.9442 | G1,G3 |
| | 2 | -2.2171±j12.6096 | 17.32 | 2.0385 | -2.3225±j11.1847 | 20.33 | 2.0351 | G2,G6 |
| | 3 | -1.3047±j10.1024 | 12.81 | 1.8108 | -1.3314±j10.3474 | 12.76 | 1.8094 | G3,G5 |
| | 4 | -0.9248±j8.5641 | 10.74 | 1.6512 | -0.9321±j8.5509 | 10.84 | 1.6515 | G5,G7 |
| | 5 | -0.8997±j9.0215 | 9.92 | 1.3694 | -0.9210±j10.3444 | 8.87 | 1.3673 | G4,G5 |
| | 6 | -0.6389±j7.1762 | 8.87 | 1.1453 | -0.6441±j7.1671 | 8.95 | 1.1481 | G7,G8 |
| | 7 | -0.1425±j3.1791 | 4.48 | 0.6652 | -0.1657±j3.1874 | 5.19 | 0.6665 | G6,G7 |

Comparing Table 2 and Table 6, it can be seen that when the CP is reduced, the eigenvalues and damping ratios related to the system low frequency oscillation modes have increased a little, but the effect is not significant. Among them, the eigenvalues of oscillation modes 2, 4 and 5 have the largest increase, and the damping ratios are increased by about 1%. The eigenvalues of the other modes have a very limited increase. When increasing the CP, the eigenvalues and damping ratios of the system mostly decrease slightly, which is not conducive to the small signal stability of the system. Among them, the eigenvalue reduction amplitude of oscillation mode 5 is the largest, the reduction amplitudes of oscillation modes 1 and 3 are similar, the reduction amplitude of oscillation modes 2 and 7 are close, and only the eigenvalue of oscillation mode 4 is improved. Through multi-controller parameters optimized, it can be seen that whether it is to increase CP or decrease CP, the eigenvalues of the system under low frequency oscillation modes are effectively improved. Among them, the eigenvalues corresponding to modes 1, 2 and 3 have the largest increase, and the damping ratio can be increased by 7%. The weak eigenvalue λ7 of mode 7 has been significantly improved, and the damping ratio is about 5 times that of the initial value. This shows that the proposed ELM-SDA can effectively improve eigenvalues and damping ratios under the low frequency oscillation modes of the system, and enhance the small signal stability of the system.

In order to further analyse the stability of the system in the dynamic time-domain, the same three-phase short-circuit fault is applied to the power system. After changing the CP of UPFC-PODC, the power angle and active power response curves of the system are shown in Figure 12 and Figure 13.

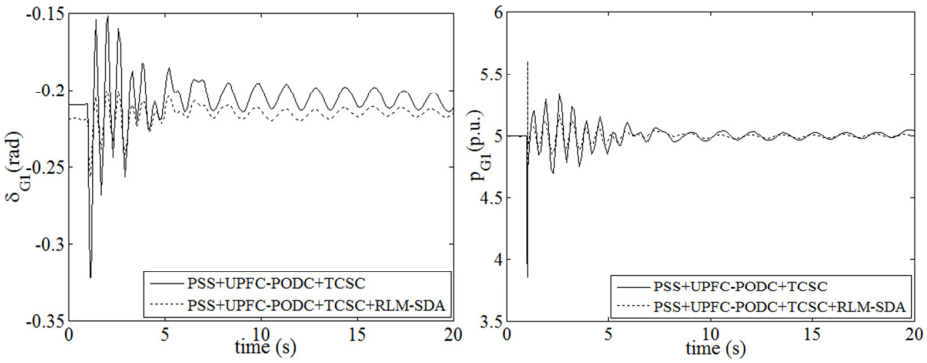


**Figure 12** δ and P response curves of Case 3

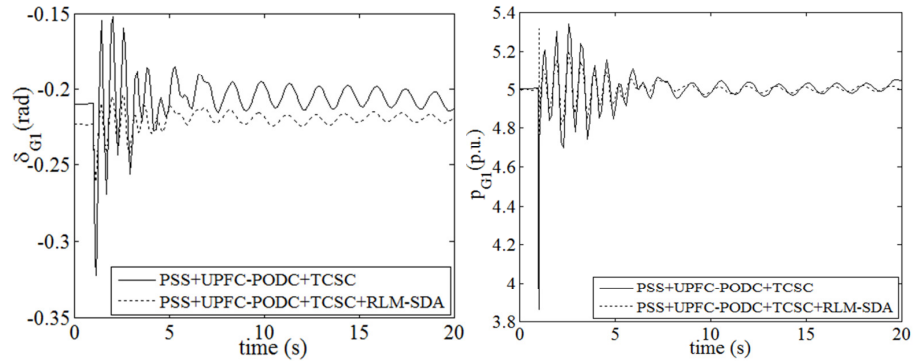


**Figure 13** δ and P response curves of Case 4

From the response curves of Figure 12 and Figure 13, it can be clearly found that when the CP of UPFC-PODC is reduced, the anti-interference ability of the system will be enhanced. When the system encounters a short-circuit fault, the power angle and active power oscillation amplitudes of the system is reduced to a certain extent. By optimizing the parameters of PSS, TCSC and UPFC-PODC, the oscillation amplitudes of active power of the system can be further suppressed, and it takes less time to restore stability. In addition, by comparing oscillation curves of the system, it is found that the proposed ELM-SDA can provide sufficient additional damping for the low frequency oscillation of the system, improve the overall damping level of the system, and enhance the small-signal stability of the system.

## 7. Conclusion

The integration of large-scale wind farms and photovoltaic stations in power systems brings a wider distribution of system eigenvalues, which is not conducive to the dynamic stability of the system. This paper aims to improve the overall damping level of the wind-PV grid-connected power generation system, and proposes an improved steepest descent method ELM-SDA, which realizes the coordinated design of PSS, TCSC and UPFC-PODC

parameters, and improves the stability of the system. In order to further improve the calculation efficiency and accuracy of the SDA, the initial values and value ranges of the parameters to be optimized are determined according to the movement trend of the eigenvalue locus. Then an objective function based on eigenvalue and damping ratio is constructed, the parameter optimization problem is transformed into an extreme value problem of the objective function, and the SDA is used to achieve coordinated optimization of parameters to maximize the damping level of the system in low frequency oscillation modes. Finally, using the eigenvalue analysis and dynamic time-domain simulation method, the proposed ELM-SDA is verified in an 8-machine 24-bus system.
The simulation results verify the effectiveness of the proposed ELM-SDA in solving PSS and multi-type FACTS devices parameters optimization problems. The coordinated design of PSS, TCSC and UPFC-PODC gain parameters can significantly improve the overall damping level of the wind-PV grid-connected system, enhance the system's anti-interference ability, and the small signal stability of the system is effectively improved.

## Acknowledgment

This work is jointly supported by the National Natural Science Foundation of China (NSFC) (No. 51607158), the Scientific and Technological Research Foundation of Henan Province (No. 222102320198), and the Key Project of Zhengzhou University of Light Industry (No. 2020ZDPY0204).

## References

[1] A. Qazi, F. Hussain, N. A. Rahim and et al. Towards Sustainable Energy: A Systematic Review of Renewable Energy Sources, Technologies, and Public Opinions. IEEE Access. 2019; 7: 63837-63851.
[2] E. Omar, H. Abu-Rub and F. Blaabjerg. Renewable energy resources: current status, future prospects and technology. Renewable and sustainable Energy Reviews. 2014; 39: 748–764.
[3] X. Fang, J. Yao, R. K. Liu and et al. Small-Signal Stability Analysis and Current Control Reference Optimization Algorithm of DFIG-Based WT During Asymmetric Grid Faults. IEEE transactions on power electronics. 2021; 36(7): 7750-7768.
[4] S. K. Tiwari, B. Singh and P. K. Goel. Design and Control of Autonomous Wind–Solar System With DFIG Feeding 3-Phase 4-Wire Loads. IEEE Transactions on industry applications. 2018; 54(2): 1119-1127.
[5] Y. Lin, L. L. Fang and Z. X. Miao. Wind in Weak Grids: Low-Frequency Oscillations, Subsynchronous Oscillations, and Torsional Interactions. IEEE Transactions on power systems. 2020; 35(1): 109-118.
[6] L. Sun, K. Liu, J. B. Hu and Y. H. Hou. Analysis and Mitigation of Electromechanical Oscillations for DFIG Wind Turbines Involved in Fast Frequency Response. IEEE Transactions on power systems. 2019; 34(6): 4547-4556.
[7] S. R. Paiyal, P. K. Ray, S. R. Mohanty and et al.. An adaptive fractional fuzzy sliding mode controlled PSS for transient stability improvement under different system uncertainties. IET smart grid. 2021; 4 (1): 61–75.
[8] A. K. Gupta, K. Verma and K. R. Niazi. Robust coordinated control for damping low frequency oscillations in high wind penetration power system. International Transactions on Electrical Energy Systems. 2020; 119(3): 105877.
[9] J. Bhukya and V. Mahajan. Mathematical modelling and stability analysis of PSS for damping LFOs of wind power system. IET Renewable Power Generation. 2020; 13(1):103-115.
[10] A. G. Tan, Z. H. Tang, X, B, Sun and et al.. Genetic Algorithm-Based Analysis of the Effects of an Additional Damping Controller for a Doubly Fed Induction Generator. Journal of Electrical Engineering & Technology. 2020; 15(4): 1585-1593.
[11] N. Nahak, S. Bohidar and R. K. Mallick. Identification of Critical Wind Farm Locations for Improved Stability and System Planning. International Journal of Energy Research. 2020; 10(4): 1907-1918.
[12] A. Mohanty, S. Patra and P. K. Ray. Robust fuzzy-sliding mode based UPFC controller for transient stability analysis in autonomous wind-diesel-PV hybrid system. IET Generation Transmission & Distribution. 2016, 10(5), pp. 1248-1257.
[13] H. H. Kuang, L. P. Zheng, S. Q. Li and X. W. Ding. Voltage stability improvement of wind power grid-connected system using TCSC-STATCOM control. IET Renewable Power Generation. 2018; 13(2): 215-219.
[14] M. Deepak, R. J. Abraham, F. M. Gonzalez-Longatt and et al. A novel approach to frequency support in a wind integrated power system. Renewable energy. 2017; 108: 194-206.

[15] M. Shafiullah, M. J. Rana, M. S. Shahriar and M. H. Zahir. Low-frequency oscillation damping in the electric network through the optimal design of UPFCcoordinated PSS employing MGGP. Measurement. 2019; 138: 215-219.
[16] S. H. Li, H. Zhang and Y. K. Li. Optimization to POD parameters of DFIGs based on the 2nd order eigenvalue sensitivity of power systems. IET Generation, Transmission & Distribution. 2021; 15(7): 1123-1135.
[17] A. Sabo, N. I. A. Wahab, M. L. Othman and et al. Optimal design of power system stabilizer for multimachine power system using farmland fertility algorithm. 2020; 30(12):1-33.
[18] A. H. Naghshbandy and A. Faraji. Coordinated design of PSS and unified power flow controller using the combination of CWT and Prony methods with the help of SPEA II multi-objective optimisation algorithm. 2019; 13(21): 4900-4909.
[19] J. Bhukya and V. Mahajan. Optimization of damping controller for PSS and SSSC to improve stability of interconnected system with DFIG based wind farm. Electrical Power and Energy Systems. 2019; 108: 314-355.
[20] G. Z. Zhang, W. H. Hu, D. Cao and et al.. A data-driven approach for designing STATCOM additional damping controller for wind farms. Electrical Power and Energy Systems. 2020; 117: 105620-105633.
[21] P. Gupta, A. Pal and V. Vittal. Coordinated Wide-Area Control of Multiple Controllers in a Power System Embedded With HVDC Lines. IEEE Transactions on Power Systems. 2021; 36(1): 648-658.
[22] S. C. Liu, X. P. Liu and X. Y. Wang. Stochastic Small-Signal Stability Analysis of Grid-Connected Photovoltaic Systems. IEEE Transactions on Industrial Electronics. 2016; 63(2): 1027-1038.
[23] J. Tanner and K. Wei. Low rank matrix completion by alternating steepest descent. Applied and Computational Harmonic Analysis. 2016. 40(2): 417-429.
[24] P. Kundur, N. J. Balu and M. G. Lauby. Power system stability and control. New York: McGraw-Hill; 1994, 139-166 p.
[25] P. He, F. S. Wen, G. Ledwich, Y. S. Xue and K.W. Wang. Effects of Various Power System Stabilizers on Improving Power System Dynamic Performance. International Journal of Electrical Power & Energy Systems. 2013; 46(1): 175-183.